Chapter 4

Mechanism of Microstructure Evolution for the Cu/Ta/GaAs Structure after Thermal Annealing

---

In this chapter, the diffusion behavior and microstructure evolution of Cu/Ta/GaAs multilayers after thermal annealing are investigated and the mechanism is proposed. X-ray diffraction analysis, Auger electron spectroscopy, high-resolution trasmission electron microscopy (HRTEM), X-ray energy dispersive spectroscopy (EDS), fast Fourier transformation (FFT) were used to identify the phases and interfaces.

4.1 Introduction

With the rapid development of the high-frequency communication industry, GaAs integrated circuits have become very important for wireless commonication applications. Traditionally, GaAs field-effect transistors (FETs) and monolithic microwave integrated circuits (MMICs) use Ti as the adhesion layer, and Au as the metallization metal for transmission lines, inductors and ground plane metallization. Using copper in place of gold as the metallization metal for the GaAs devices has the advantages of low resistivity, high thermal conductivity and low cost. Moreover, if Au is replaced with Cu for frontside transmission lines, the electrical conductivity can be

improved to increase the speed.

Copper diffuses very fast into silicon if no diffusion barrier is used. [1-3] It is generally confirmed that the rapid diffusion results from singly ionized interstitial copper which migrates as a positively charged ion in silicon.[4] Similarly, copper is known to diffuse rapidly into GaAs via a kick-out mechanism if no diffusion barrier is used[5-8] and creates deep traps that degrade the device characteristics.[9-10] Recently, the thermal stability of Cu/Ta/Si has been studied vigorously and Ta has been proved to be an effective diffusion barrier for Cu metallization in Si technology because of its immiscibility with Cu.[11-13] Therefore, it is worthwhile to study the feasibility of Cu metallization on GaAs devices using a Ta barrier.

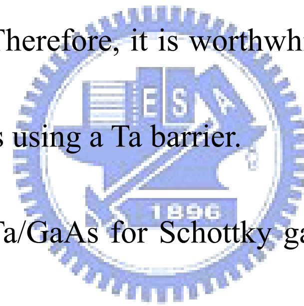

The thermal stabilities of Ta/GaAs for Schottky gate use have been reported with experimental results[14-20] and theoretical thermodynamics-based calculations.[21-22] Moreover, the electrical properties of the Cu/Ti/GaAs structure for Schottky gate use[23] or of Cu/GaAs for ohmic contact use[24] have also been reported. However, the thermal stability of the Cu/Ta/GaAs multilayers for backside-surface and transmission line metallization has never been studied. We previously reported[25] that a sputtered Ta film effectively prevented the interaction of Cu and GaAs after annealing at temperatures of up to 500 °C. We also reported that MESFET metallization using Cu/Ta layers exhibited good power performance and thermal conductance and

demonstrated excellent thermal stability after thermal stress.[26,27] In this paper, we extend the previous work to characterize the diffusion behavior and microstructure evolution of the Cu/Ta/GaAs structure with thermal annealing.

4.2 Experimental procedure

Before metal film deposition, the backside of 3 in. GaAs(100) substrates was deposited with 100 nm Si_3N_4 to avoid outdiffusion of As during the annealing process. The substrates were then cleaned with boiling acetone and isopropyl alochol for 5 min, followed by dipping with $HF:H_2O_2:H_2O$ (1:2:20) for 20 s and $HCl:H_2O$ (1:4) for 1 min. The metal films were deposited by sputtering in a multi target dc magnetron sputtering system. A tantalum film of 30 nm thickness was first sputtered on top of the GaAs substrate, then a 100 nm Cu film and a 10 nm tantalum nitride film were subsequently sputtered on top of the Ta film without breaking the vaccum. Note that for the test samples, a top tantalum nitride (10 nm) layer was deposited on the surface of Cu to protect the copper layer from oxidation. The samples were annealed for 30 min at temperatures ranging from 400 to 600 °C in argon ambient. The sheet resistances of the samples were measured using a four-point probe to investigate the overall reaction involving Cu. X-ray diffraction analysis (XRD) and Auger electron

spectroscopy (AES) were used to identify the phases of the reaction products and the interfacial reactions between different layers. Microstructural characterization was carried out using cross-sectional trasmission electron microscopy (TEM) with electron diffraction for phase identification, and X-ray energy dispersive spectroscopy (EDS) for microanalysis of the chemical compositions. High-resolution trasmission electron microscopy (HRTEM) was used to observe the lattice image of selected areas on the atomic scale, and the fast Fourier transformation (FFT) of the lattice images was used to identify the crystal structure patterns of the corresponding areas.

4.3 Results and Discussion

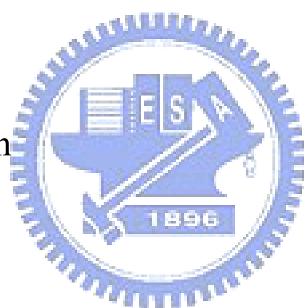

Figure 4.1 shows the sheet resistances of the samples as-deposited and after 400-600 °C annealing. The sheet resistance of the Ta_2N/Cu/Ta/GaAs film structure as-deposited was 0.275 Ω/□; if initially dropped to 0.255 Ω/□ after 400°C annealing and dropped to 0.240 Ω/□ after 500 °C annealing, which is apparently due to the grain growth and decrease in defect density in the Cu and Ta films after annealing. The sheet resistance increased slightly after annealing at 550 °C to 0.330 Ω/□, which implies that diffusion and/or the emergence of a more resistive compound might have occurred. After annealing at 600 °C, the sheet resistance

markedly increased to 5.5 Ω/□, suggesting that a severe inter diffusion occurred between the layers.

To clearly understand the correlation between the sheet resistance and the microstructure formed, XRD and TEM were used to identify the phases and observe the microstructures formed. Figure 4.2 shows the XRD results of the Ta_2N/Cu/Ta/GaAs samples as-deposited and after annealing at various temperatures. The peaks of Ta can be indexed as (002) and (004) of β-Ta. From the XRD data, it is clear that the peaks of Ta and Cu almost remain unchanged after 500 °C annealing, suggesting that the Cu/Ta/GaAs structure is still stable up to 500 °C. After annealing at 550 °C, additional peaks with peak overlap were found, these peaks were identified as $TaAs_2$ and Cu_3Ga peaks. Formation of the phases of $TaAs_2$ and Cu_3Ga implies that inter diffusion occurred in the multilayer structure after annealing at 550 °C. It is consistent with the increase in sheet resistance after annealing at 550 °C. However, after annealing at 600 °C, the peaks of Cu and Ta disappeared, and peaks identified as TaAs and Cu_3Ga compound appeared, implying that significant inter diffusion reactions occurred among these layers. These results explain the marked increase in sheet resistance after annealing at 600 °C. As can be seen from Fig. 4.2, the Ta_2N peak at 38.6^o can be found from all the annealed samples except for the 600 °C-annealed one, suggesting that the Ta_2N protective layer on the top of the Cu layer

was ineffective at 600 °C.

Additional evidence showing the stability of the multilayer structure after annealing at 500 °C can be obtained from the AES depth profiles in Fig. 4.3. As can be seen from these figures, the distribution of the elements in the deposited films remained almost unchanged after annealing at 500 °C; however, annealing at higher temperatures (above 550 and 600 °C) results in severe redistribution of all the elements in the multilayer.

Figure 4.4(a) shows a cross-sectional TEM micrograph of the Ta_2N/Cu/Ta/GaAs structure under the as-deposited condition. The thin-film structure is uniform with very sharp interfaces between each layer, and there is no diffusion reaction or intermixing. The as-deposited Cu film has an average grain size of 50-60 nm. Figure 4.4(b) shows a high-resolution TEM image obtained from the same sample further thinned to a smaller thickness, revealing that the microstructure of the Ta layer is of a nano crystalline phase without preferred orientation for the Ta grains. Figures 4.4(c) and 4.4(d) show lattice images of the Ta crystal and its FFT pattern, from which the Ta can be indexed as the beta phase. In Fig. 4.4(b), a thin TaO_x layer formed between Ta and Cu can also be found. This oxidation layer is often observed when Ta and Cu are thin enough, probably owing to the oxidation of Ta film when the TEM specimen was exposed to air for more than a few days. Such a TaO_x layer was also formed in

the $Cu/Ta/SiO_2/Si$ structure as reported by Yin et al.[28,29] In Fig. 4.5, after annealing at 500 °C, grain growth of the Cu and Ta occurred, and there was no evidence of intermixing of the Cu and Ta with the GaAs substrate. The Ta grains were in a columnar structure perpendicular to the GaAs substrate. The Cu grains were large enough to span the space between Ta_2N and Ta layers.

The microstructure of the sample annealed at 550 °C is shown in Fig. 4.6. It is found that some extra compounds with triangle and semi sphere shapes formed on both sides of the Ta layer. A detailed examination shows that these compounds are $TaAs_2$ and Cu_3Ga. Figure 4.6(a) shows the microstructure around the Ta interfaces. The particle with a triangle shape is located beneath the Ta layer, while a bumped particle is on top of the Ta. Figure 4.6(b) shows an enlarged image of the reaction area at the Ta/GaAs interface. The lattice image of the particle in Fig. 4.6(c) with its FFT pattern in Fig. 4.6(d) shows that it is monoclinic $TaAs_2$, with a = 0.935, b = 0.3388, and c = 0.7760 nm.[30] The $(31\bar{3})$ plane of $TaAs_2$ is parallel to the {111} plane of GaAs. A high-resolution TEM image of the reaction area at the Cu/Ta interface opposite to the location of $TaAs_2$ is shown in Fig. 4.6(e) with a lattice image of the particle in Fig. 4.6(f) and its FFT pattern in Fig. 4.6(g). The structure of the particle is identified as hexagonal Cu_3Ga, with a = 0.2600 and c = 0.4229 nm.[30] Parallel formation of $TaAs_2$ and Cu_3Ga on each side of the Ta layer is unusual. The reaction of

Ta with As to form $TaAs_2$ is likely to release Ga from GaAs. The released Ga can then diffuse through the Ta layer along the shortest path to the Cu side to form Cu_3Ga at the Cu/Ta interface as observed in the TEM images. These results clearly show that Ga and As atoms diffused after 550 °C annealing. From the XRD results, we also found that the Ta peak shifted from that of the as-deposited sample; this is probably due to the compressive stress between the Ta layer and the GaAs substrate.

Cross-sectional TEM micrographs of the sample after annealing at 600 °C are shown in Fig. 4.7. Figures 4.7(a) and 4.7(b) are taken from different regions of the same sample. It is clearly seen that the Ta layer disappeared, while a large number of reaction particles scattered around the specimen. The total thickness of the reaction regions above the GaAs substrate is over 200 nm, which is larger than the deposited Cu and Ta thickness. This is indicative of the occurrence of disrupted reactions at this temperature. Moreover, it is noticed that large semi sphere-shaped diffusion zones were formed in the GaAs substrate at some intervals along the Ta/GaAs boundary. The zone in Fig. 4.7(a) has a size about 600 nm, while that in Fig. 4.7(b) has a size larger than 1500 nm. After careful examination of Figs. 4.7(a) and 4.7(b), it is found that no particles formed in the large semi sphere-shaped diffusion zone as shown in Fig. 4.7(a), but many particles formed in the large reaction zone as shown in Fig. 4.7(b). Figure 4.7(c) shows an enlargement of a section from Fig. 4.7(b). The

selected-area diffraction (SAD) patterns from the areas in Fig. 4.7(c) are shown in Figs. 4.7(f) and 4.7(g); only two different kinds of phases can be identified from these patterns. One is TaAs, and the other is Cu_3Ga. Figures 4.7(d) and 4.7(e) show the corresponding dark-field images taken from the diffraction spots of the TaAs and Cu_3Ga phases, respectively. From the images, we can see that the darker particles in the bright-field image are normally TaAs due to their heavier atomic mass. These particles formed not only at the interface with GaAs, but also precipitated in the initially deposited Cu layer. The lighter particles are Cu_3Ga, mainly formed in the zones and the Cu layer. Figures 4.8(a)-4.8(c) show the EDS spectra taken from sites A-C in Fig. 4.7(a), and Fig. 4.8(d) shows the EDS taken from site D in Fig. 4.7(b). Figure 4.8(a) shows a high concentration of Cu in the diffusion zone with Ga and As atoms dissolved. It is reasonable to see the dissolution of Ga and As atoms in the Cu layer because the solubility of Ga and As in Cu increased with increasing annealing temperature according to the Cu-Ga and Cu-As phase diagrams. Therefore, it is suggested that the diffusion zone is caused mostly by the diffusion of Cu atoms. Figure 4.8(b) was taken from the TaAs phase, which contains mostly Ta and As atoms. Figures 4.8(c) and 4.8(d) show the EDS spectra from the lighter areas; the spectra show that these areas contain mostly Cu and Ga atoms. It is not certain whether the presence of the small amount of As and Ta in the Cu_3Ga phase is brought about the

beam-broadening effect from adjacent areas or whether they are genuinely dissolved in the phase. From the above results, the reaction sequence of the Cu/Ta/GaAs multilayer after high-temperature annealing can be summarized as follows. The first step may be the reaction of Ta with As to form TaAs at the Ta/GaAs interface; this is because TaAs appeared all over the structure along the Ta/GaAs interface despite the large semi sphere-shaped diffusion zone formed. The large number of TaAs grains destroyed the continuity of the Ta layer, which then caused the rapid diffusion of Cu through the unstable Ta layer into the GaAs substrate to form the semi sphere-shaped diffusion zone. Once As diffused, a large part of the GaAs interface turned out to be depleted of As atoms, and it is possible for Ga to diffuse out toward the interface. As a result of the out-diffusion of Ga atoms, Cu_3Ga grains started to form at the regions near the interface. As annealing time increased, interactions of Cu and Ta with GaAs proceeded, resulting in the precipitation of Cu_3Ga particles with TaAs particles in the diffusion zone.

For the case of Cu and GaAs separated by a 30 nm sputtered Ta film, the mechanism explaining why the barrier fails at about 550 °C is the reaction of Ta and GaAs to form $TaAs_2$, and the diffusion of Ga atoms through the Ta layer to form Cu_3Ga. However, for the case of 600°C annealing, Ta reacts with GaAs to form TaAs, followed by the mass diffusion of all elements and results in the failure of the Ta barrier. The difference in behavior between 550 and 600 °C annealing can be explained by the thermodynamic consideration of the phases observed. Studies on the

thermal stability of Ta/GaAs contact have been reported. Lahav and Eizenberg[15] showed that a 100-nm-thick Ta layer on GaAs annealed for 1 h had only a slight interaction at 600 °C, while after 650 °C annealing, the film fully reacted to form a Ta_3Ga_2/TaAs/GaAs structure. Huang and Jean[19] reported that an extensive reaction of a 100-nm-thick Ta layer with GaAs after 700 °C rapid thermal annealing resulted in the formation of TaAs, $TaAs_2$, and Ta_3Ga_2 phases. The above reports show various results regarding the phase stabilities at different temperatures due to different kinds of sample preparation with different annealing methods. Although the interpretation of these results is difficult due to the complexity of gallium-arsenic-metal interactions and the lack of experimental thermodynamic data, a common conclusion can still be drawn; i. e., TaAs is the most stable phase, and the $TaAs_2$ phase is less stable and decomposes into the TaAs phase at higher temperatures. Similar results are also reported by Niessen[30] with theoretical calculations, showing that the enthalpies of formation of the compounds TaAs and $TaAs_2$ are –90 and –71 kJ/mole, respectively. The observations in this study that the formation of $TaAs_2$ at 550 °C and that the formation of the TaAs phase occurred at 600 °C are in good agreement with the results of theoretical considerations of the energy of formation. In the current cases, $TaAs_2$ is a metastable phase. However, the formation of $TaGa_2$ at 550 °C seems to occur at lower temperature than in the other reports.

Due to the formation of $TaAs_2$, the released Ga atoms penetrate through the Ta layer to form Cu_3Ga at the opposite sides of the Ta layer. The sequence and morphology of the Cu/Ta/GaAs multilayer after thermal annealing are different from those of the Cu/Ta/Si multilayer after thermal annealing; in the latter case, the barrier failure is caused by the diffusion of Cu through the Ta layer to form Cu_3Si at the Ta/Si interface, and Ta reacts with Si to form $TaSi_2$ at higher temperatures.[28]

4.4 Conclusions

The diffusion behavior and microstructure evolution of Cu/Ta/GaAs multilayers after thermal annealing are investigated and the mechanism is proposed. A thin 30 nm tantalum layer was sputtered as a diffusion barrier to block Ga and As diffusion into the Cu layer. From the results of sheet resistance measurement, X-ray diffraction analysis, Auger electron spectroscopy and transmission electron microscopy, the Cu/Ta films on GaAs were found to be very stable up to 500 °C without Cu migration into GaAs. After annealing at 550 °C, the interfacial mixing of Ta with GaAs substrate occurred, resulting in the formation of $TaAs_2$, and the diffusion of Ga through the Ta layer formed the Cu_3Ga phase at the Cu/Ta interface. After annealing at 600 °C, the reaction of GaAs with Ta and Cu formed TaAs and Cu_3Ga owing to Ga migration and interfacial instability.

4.5 References

1) E. R. Weber: Appl. Phys. A **30** (1983) 1.

2) A. Cros, M. O. Aboelfofotoh, and K. N. Tu: J. Appl. Phys. **67** (1990) 3328.

3) C. A. Chang: J. Appl. Phys. **67** (1990) 566.

4) C. S. Fuller and J. C. Severiens: Phys. Rev. **96** (1954) 21.

5) R. N. Hall and F. H. Racettte: J. Appl. Phys. **35** (1964) 379.

6) P. H. Wohlbier: *Diffusion and Defect Data 10* (Trans Tech, Cleveland, 1975) p.89.

7) D. A. MacQuistan and F. Weinberg: J. Cryst. Growth **110** (1991) 745.

8) K. Somogyi, D. N. Korbutyak, L. N. Lashkevich and I. Pozsgai: Phys. Status Solidi A **114** (1989) 635.

9) R. Leon, P. Werner, K. M.Yu, M. Kaminska and E. R. Weber: Appl. Phys. A **61** (1995) 7

10) N. Kullendorff and L. Jansson: J. Appl. Phys. **54** (1983) 3203.

11) K. Holloway and P. M. Fryer: Appl. Phys. Lett. **57** (1990) 1736.

12) K. Holloway, P. M. Fryer, C. Cabral, Jr., J. M.E. Harper, P. J. Bailey, and K.H. Kelleher: J.Appl. Phys. **71** (1992) 5433.

13) D. S. Yoon, H. K. Baik, and S. M. Lee: J. Appl. Phys. **83** (1998) 8074.

14) S. D. Mukherjee, C. J. Palmstron, and J. G. Smith: J. Vac. Sci. Technol. **17** (1980) 904.

15) A. Lahav and M. Eizenberg: Appl. Phys. Lett. **46** (1985) 430.

16) A. Lahav M. Eizenberg, and Y.Komen: J. Appl. Phys. **62** (1987) 1768.

17) D. V. Morgan and J. Wood: Appl. Surf. Sci. **38** (1989) 517.

18) P. Gladkov, K. Varblianska, T. Marinova, V. Krastev, and J. Stoemenos: Appl. Surf. Sci. **59** (1992) 179.

19) T. S. Huang and S. M. Jean: J. Appl. Phys. **75** (1994) 7519.

20) Q. Han and R. Schmid-Fetzer: Mater. Sci. Eng. B **22** (1994) 141.

21) R. Beyers: J. Appl. Phys. **56** (1987) 147.

22) R. Beyers, K. B. Kim and R. Sinclair: J. Appl. Phys. **61** (1987) 2195.

23) T. Feng, A. Dimoulas, A. Christou, G. Constantinidis and Z. Hattzopoulos: Microelectron. Reliab. **37** (1997) 1699.

24) K. Sugioka and K.Toyoda: Vacuum **41** (1990) 1258.

25) C. Y. Chen, L. Chang, E. Y. Chang, S. H. Chen and D. F. Chang: Appl. Phys. Lett. **77** (2000) 3367.

26) C. Y. Chen, E. Y. Chang, L. Chang and S. H. Chen: Electron. Lett. **36** (1317) 2000.

27) C. Y. Chen, L. Chang, E. Y. Chang, S. H. Chen and Y. C. Lin: Solid-State Electron. **46** (2002) 2085.

28) K. M. Yin, L. Chang, F. R. Chen, J. J. Kai, C. C. Chiang, P. Ding, B. Chin, H. Zhang, and F. Chen: Thin Solid Films **388** (2001) 15.

29) K. M. Yin, L. Chang, F. R. Chen, J. J. Kai, C. C. Chiang, G. Chuang, P. Ding, B. Chin, H. Zhang, and F. Chen: Thin Solid Films **388** (2001) 27

1896

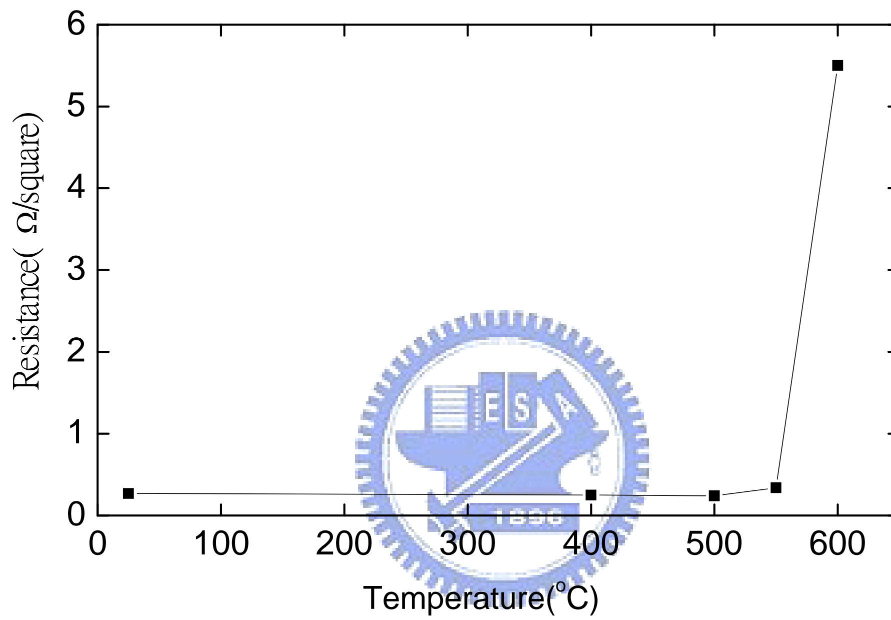

Fig. 4.1. Sheet resistances of the as-deposited sample and the samples after annealing at various temperatures.

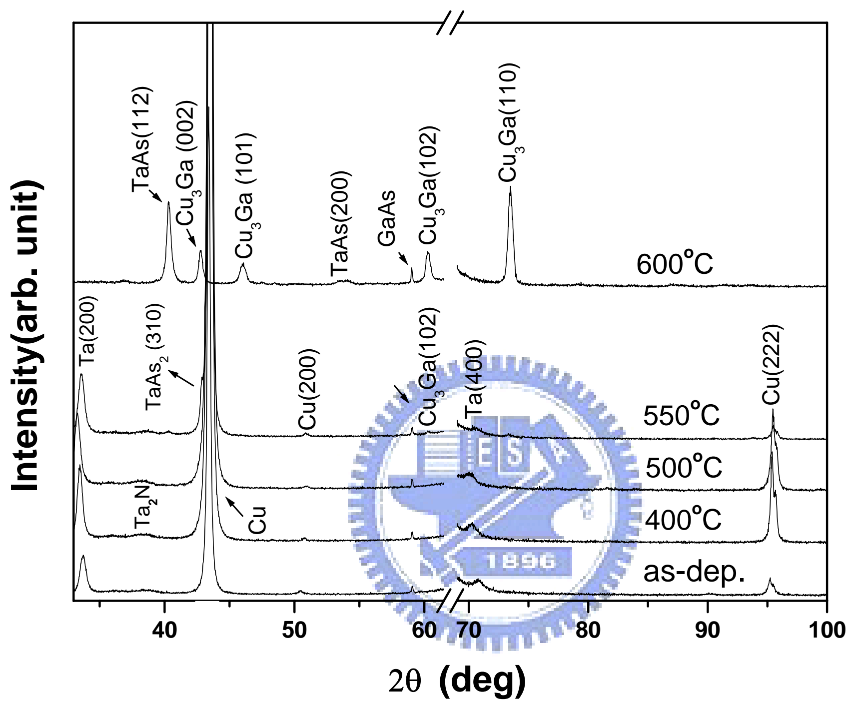

Fig. 4.2. XRD patterns of the as-deposited sample and the samples after annealing at various temperatures.

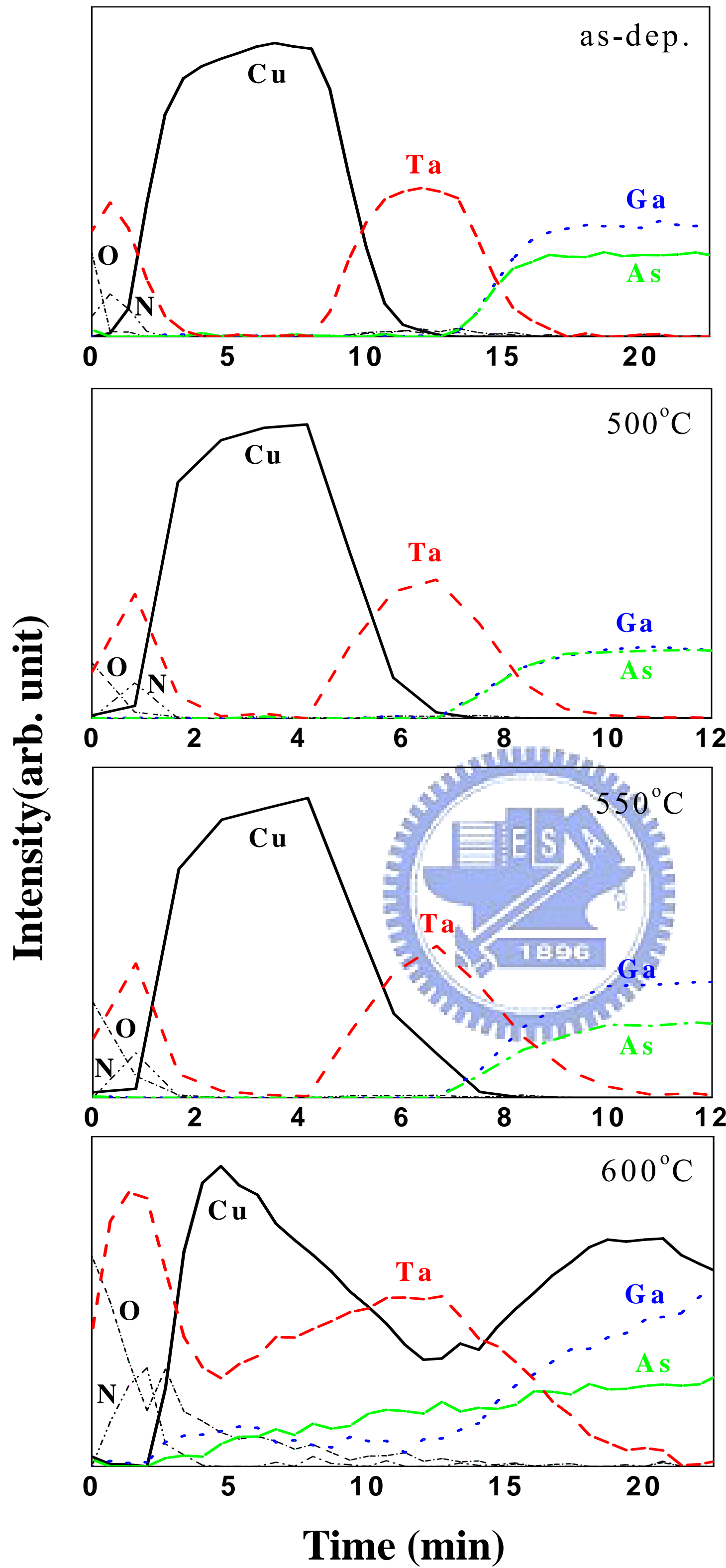

Fig. 4.3. Auger depth profiles of the as-deposited sample and the samples after annealing at various temperatures.

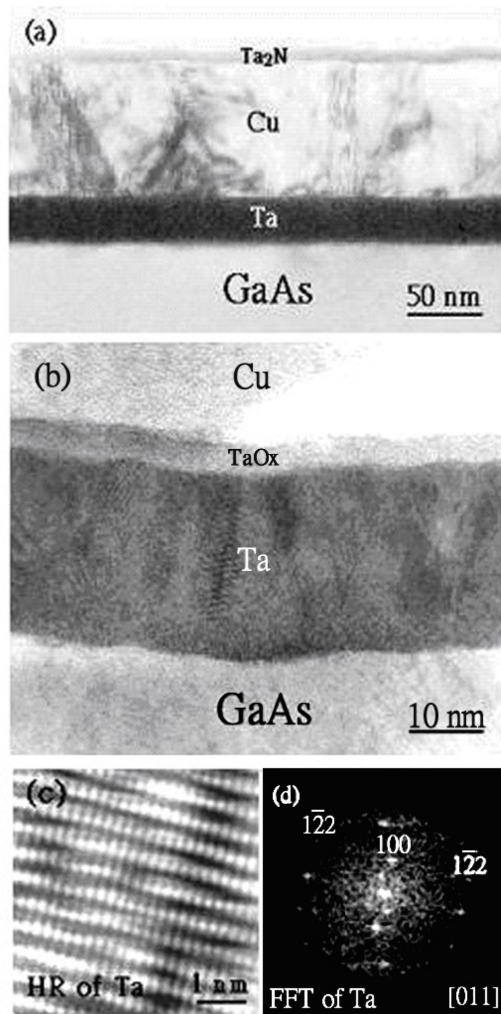

Fig. 4.4.(a) Cross-sectional TEM image of the as-deposited Ta_2N/Cu/Ta/GaAs sample. (b) High-resolution TEM image obtained from the same sample after being thinned to smaller thickness. (c) Lattice image of Ta crystal. (d) FFT pattern of Ta.

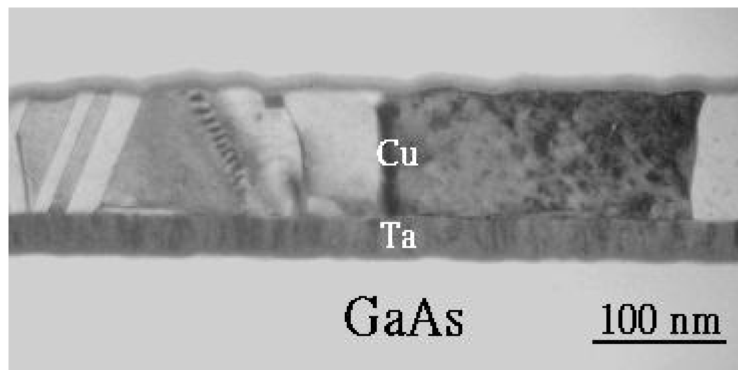

1896

Fig.4.5. Cross-sectional TEM image of the Ta_2N/Cu/Ta/GaAs sample after annealing at 500 °C for 30 min.

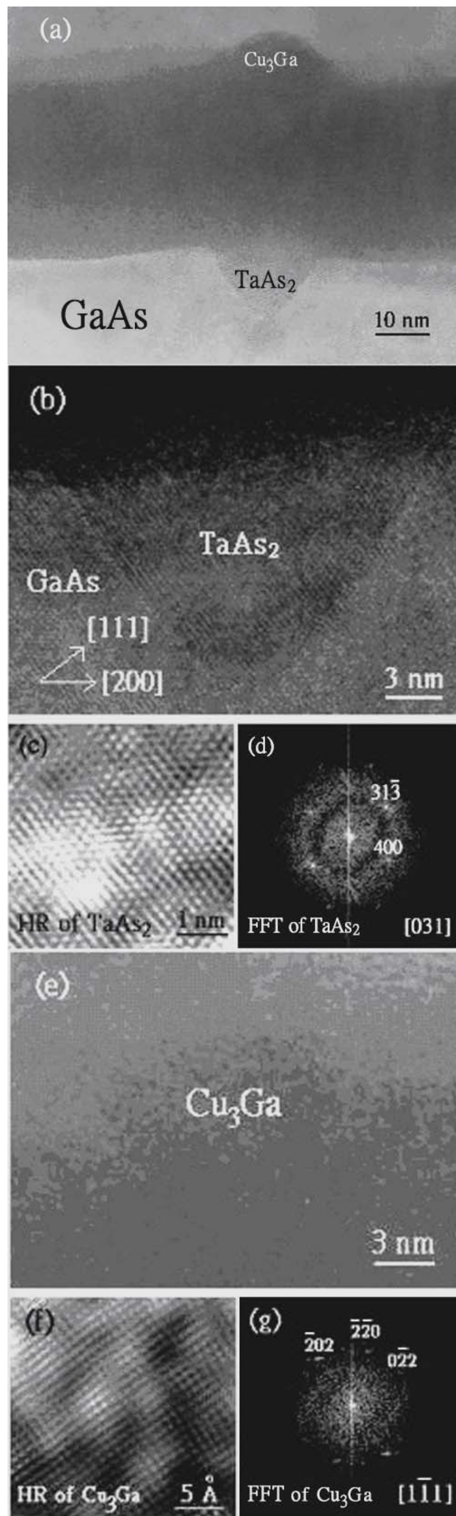

Fig. 4.6 (a) High-resolution TEM image obtained from the interface of the reaction area after annealing at 550 °C for 30 min. (b) High-resolution TEM image of the reaction area at Ta/GaAs interface. (c) Lattice image of $TaAs_2$. (d) FFT pattern of $TaAs_2$. (e) High-resolution TEM image of the reacted area at the Ta/Cu interface. (f) Lattice image of Cu_3Ga. (g) FFT pattern of Cu_3Ga grain.

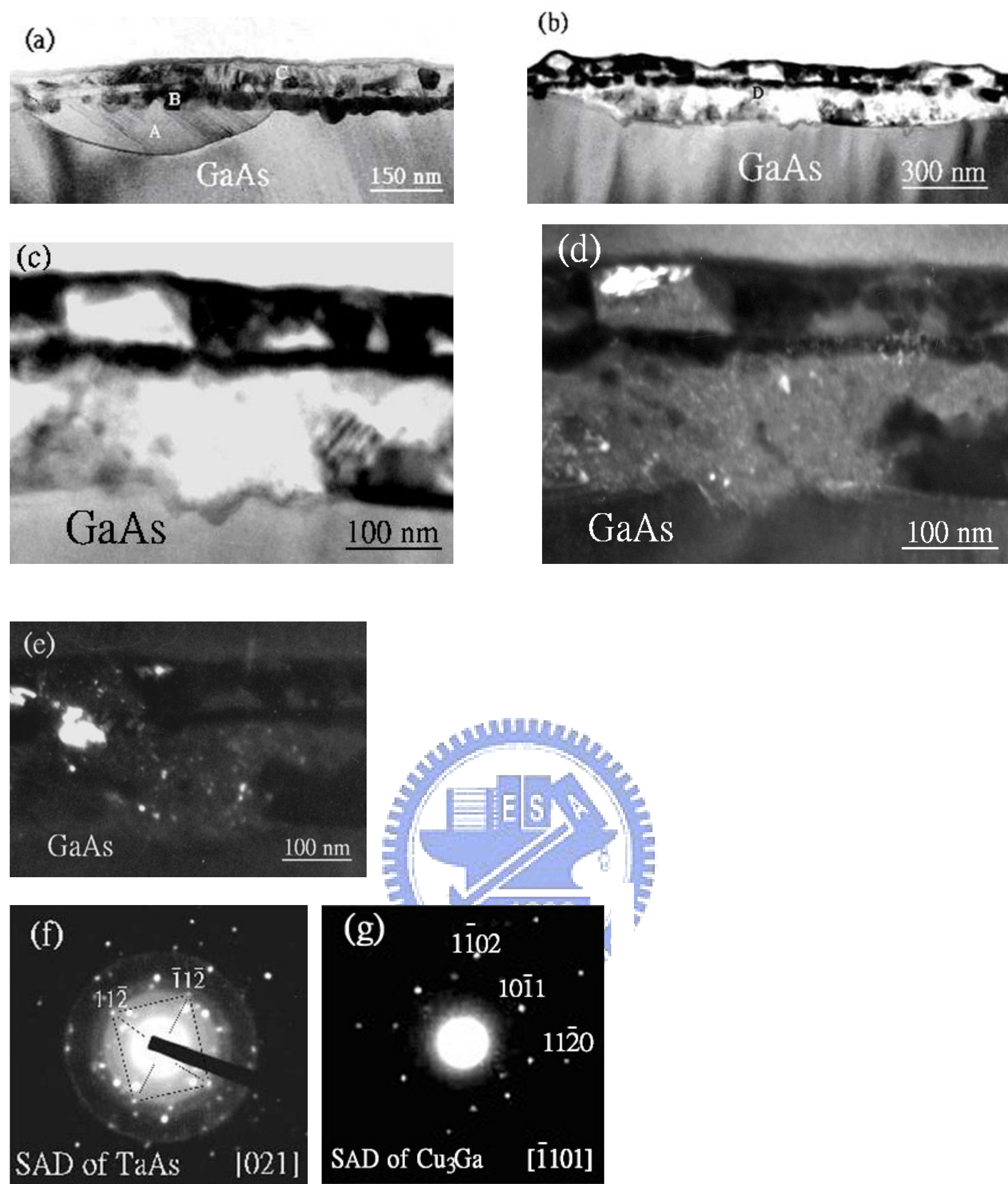

Fig. 4.7. (a) Cross-sectional TEM image of the sample after annealing at 600 °C for 30 min. (b) Cross-sectional TEM image of the same sample at another area. (c) Enlarged TEM image of an area from (b). (d) Dark-field image of TaAs. (e) Dark-field image of Cu_3Ga. (f) Selected-area diffraction pattern of TaAs. (g) Selected-area diffraction pattern of Cu_3Ga.

(a)

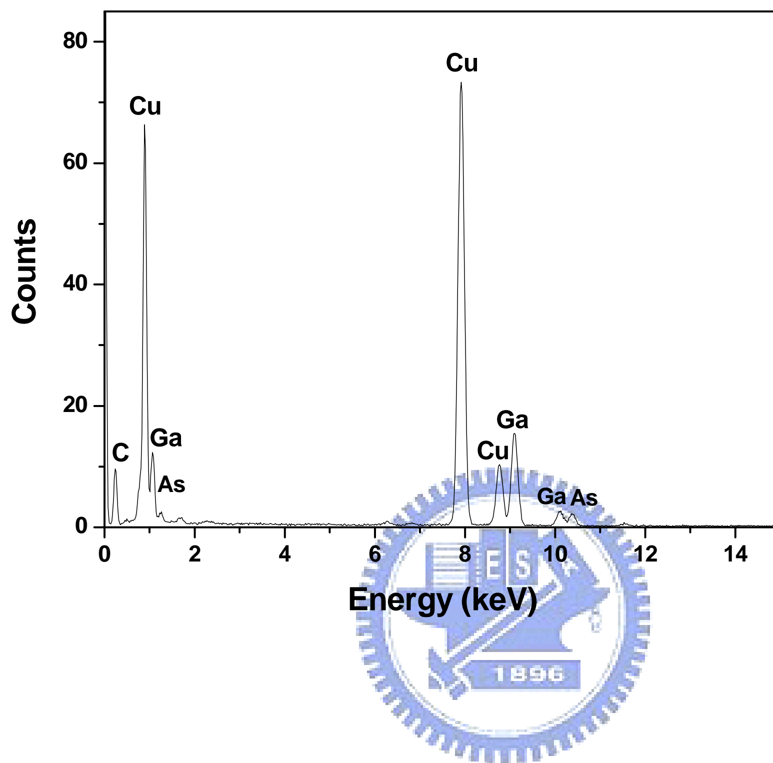

1896

(b)

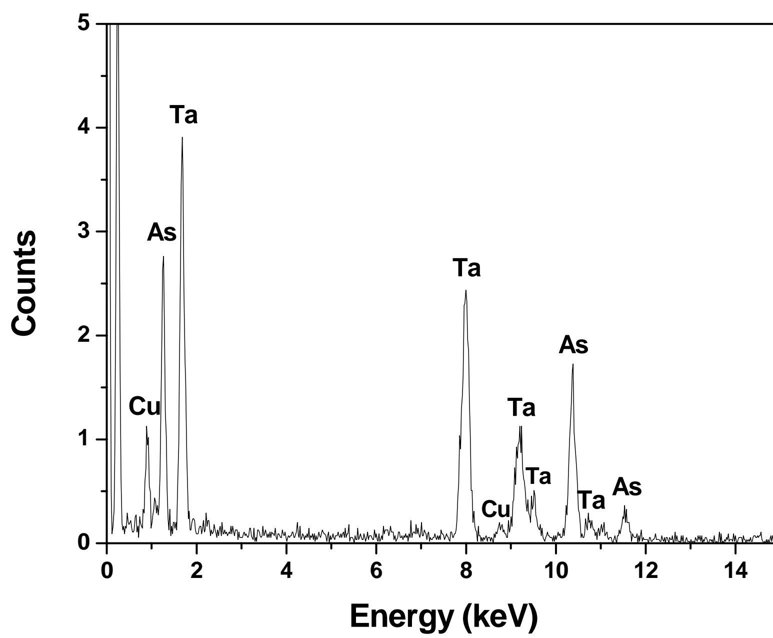

(c)

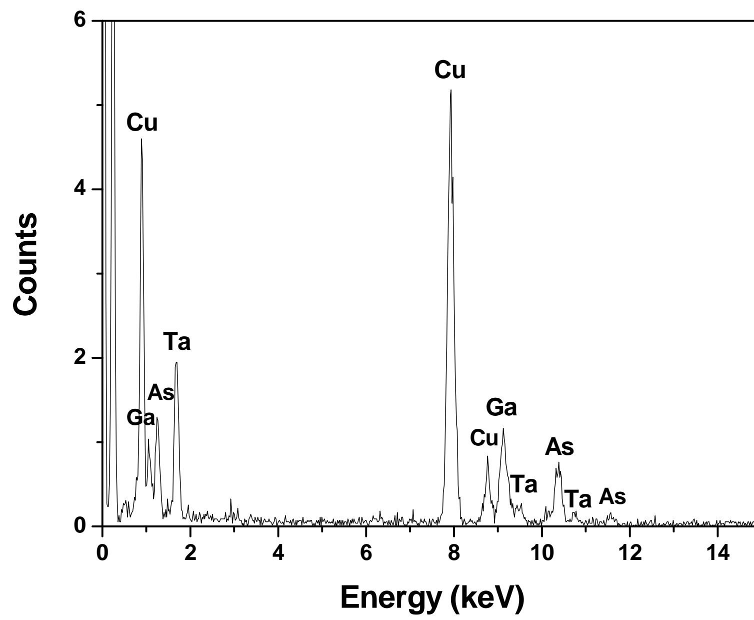

(d)

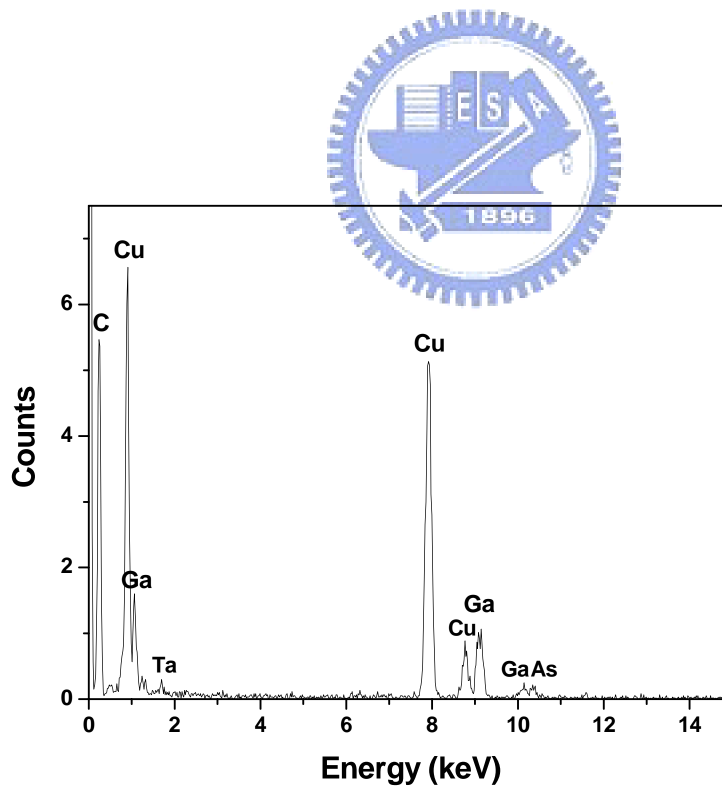

Fig. 4.8. (a)-(c) EDS spectra taken from sites A-C in Fig. 4.7(a), and (d) EDS spectrum taken from site D in Fig. 4.7(b).